Atmospheric Environment 243 (2020) 117730

Contents lists available at ScienceDirect

Atmospheric Environment

journal homepage: http://www.elsevier.com/locate/atmosenv

The importance of coal combustion and heterogeneous reaction for atmospheric nitrate pollution in a cold metropolis in China: Insights from isotope fractionation and Bayesian mixing model

Xiazhong Sun [a,b], Zheng Zong [c], Kun Wang [a,b], Bo Li [a,b], Donglei Fu [a,b], Xiaofei Shi [a,b], Bo Tang [a,b], Lu Lu [a,b], Samit Thapa [a,b], Hong Qi [a,*], Chongguo Tian [c,**]

[a] Key Laboratory of Urban Water Resource and Environment, Harbin Institute of Technology, Harbin 150090, China
[b] School of Environment, Harbin Institute of Technology, Harbin 150090, China
[c] Key Laboratory of Coastal Environmental Processes and Ecological Remediation, Yantai Institute of Coastal Zone Research,Chinese Academy of Sciences, Yantai 264003, China

HIGHLIGHTS

- Considering δ^{15} N fractionation is necessary for accurate NO_x source apportionment.
- Heterogeneous reaction played a vital role in nitrate formation in heating season.
- Coal combustion was the dominant contributor to nitrate pollution in urban Harbin.

GRAPHICAL ABSTRACT

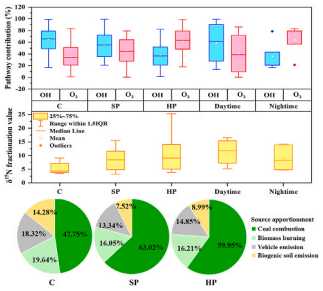

ARTICLE INFO

Keywords:
Source apportionment
Oxidation pathways assessment
Pollution levels
Heating season
Haze alleviation

ABSTRACT

Haze pollution in Harbin has been gradually alleviated in recent years, but it is still far from eliminated. Thus, precise and effective emission abatement of main chemical components like nitrate is urgently needed for further haze pollution control. This study aimed to estimate nitrate formation pathways, and the contributions of the emission sources of nitrogen oxide in urban Harbin, based on the measurement of isotope signatures in nitrate and the utilization of an improved Bayesian mixing model. The results showed that nitrate significantly aggravated particulate pollution in the heating season, and its driving role was enhanced as the pollution level increased. This study suggested that homogeneous reaction and heterogeneous reaction were the dominant conversion pathways of nitrate formation in non-heating season and heating season respectively, and the contribution of heterogeneous reaction increased as pollution levels increased. By considering isotope fractionation value (δ^{15}N), this paper emphasized coal combustion as the dominant contributor of nitrogen oxide in urban Harbin, while biomass burning, mobile sources, and biogenic soil emissions played relatively weak roles in nitrate pollution. This study has critical importance to provide scientific theoretical bases for nitrogen oxide reduction in urban Harbin and air quality improvement reference in other severely polluted regions in China.

* Corresponding author. School of environment, Harbin Institute of Technology, Harbin 150090, China.
** Corresponding author.
E-mail addresses: hongqi@hit.edu.cn (H. Qi), cgtian@yic.ac.cn (C. Tian).

https://doi.org/10.1016/j.atmosenv.2020.117730
Received 12 February 2020; Received in revised form 6 June 2020; Accepted 21 June 2020
Available online 26 August 2020

1. Introduction

In recent decades, haze pollution has become one of the most critical environmental issues in China, which was characterized by high pollutant concentration, long duration, vast region influences, adverse health effects, and considerable efforts for its removal (Zheng et al., 2015, 2016; Li et al., 2017). As the primary pollutant during haze pollution, fine particulates ($PM_{2.5}$, particles with aerodynamic equivalent diameter less than 2.5 μm) profoundly affect ecosystems and public health, such as reducing visibility and air quality, changing meteorological and climate circle, and causing respiratory system related symptoms and circulatory system diseases (Brauer et al., 2016; Lelieveld et al., 2013; Whiteman et al., 2014). Indicated from the yearly decreasing $PM_{2.5}$ concentration across China during 2013–2018, the severe haze has gradually alleviated in response to the governmental clean air action. However, it will still be a significant environmental issue in the next few years, because the mean PM2.5 concentrations in most China cities are far higher than the Chinese Ambient Air Quality Standard of 35 μg/m^3 (https://www.aqistudy.cn/historydata/about.php). Thus, accurate and effective emission reduction is urgently needed.

Many recent measurements were indicative of remarkably increasing trends and high proportions (20%–60%) of secondary inorganic aerosols (SNA: sulfate, nitrate, and ammonium) during haze evolution in China. Among which, nitrate is the most attractive, because it increased with a non-linear trend, remarkably drove the rapid build-up of $PM_{2.5}$ concentration (Zheng et al., 2016; Pan et al., 2016a,b; Fan et al., 2019), and played significant roles for haze evolution. Excessive formed nitrate mainly caused by growing nitrogen oxide (NO_x) emission and rapid secondary chemical reaction. Globally, NOx was mainly contributed by intensive anthropogenic activities. Fossil fuel burning was reported to contribute more than half ((~22.4–26.1 Tg N yr^{-1}) of the global nitrogen burden (~40 Tg N yr^{-1})). Other sources such as biomass burning emission, lighting, biogenic soil emission contributed to the remainder part (Gu et al., 2012, 2015). The secondary chemical reaction of nitrate mainly involved the rapid transformations of nitric oxide (NO) and nitrogen dioxide (NO_2) (R1–R2), and the oxidation reactions from NO_x to nitric acid (HNO_3) through homogeneous (R3: NO_2 + OH) and heterogeneous (R4–R6: N_2O_5 + H_2O) reactions (Vienne et al., 1961). The results of theoretical simulation showed that nitrate oxidized by hydroxyl (OH) radical and ozone (O_3) respectively involved nearly 76% and 18% of nitrate formation (Alexander et al., 2009), and are regarded as primary oxidation pathways for nitrate formation. Both nitrate and NO_x were reported to have negative effects on haze alleviation. Nitrate in fine mode can degrade visibility, absorb liquid water, enhance particle hygroscopicity, and promote SNA formation (Pan et al., 2016a,b; Wang et al., 2017). Moreover, its precursors, NO_x was believed to have a crucial function in promoting the formation of atmospheric oxidants (O_3, OH) and secondary aerosol, profoundly affect the self-cleansing capacity of the atmospheric environment (Galloway et al., 2003; Xiao et al., 2015). A simulation by Liu et al. (2019) using WRF-Chem showed that the concentrations of particulate ammonium nitrate decrease by 30%–60% relative to the baseline levels could contribute approximately 70% of $PM_{2.5}$ mass reduction in China (Liu et al., 2019). This finding above further promoted our understanding of the importance of nitrate. It also provided evidence that control nitrate formation and NO_x emission have profound significance in establishing positive feedback of secondary reaction prevention and haze alleviation.

$$NO_{(g)} + O_{3(g)} \rightarrow NO_{2(g)} + O_{2(g)} \quad (R1)$$

$$NO_{2(g)} + h\nu \rightarrow NO_{(g)} + O \quad (R2)$$

$$NO_{2(g)} + OH \rightarrow HNO_{3(g)} \quad (R3)$$

$$NO_{2(g)} + O_{3(g)} \rightarrow NO_{3(g)} + O_{2(g)} \quad (R4)$$

$$NO_{3(g)} + NO_{2(g)} \rightarrow N_2O_{5(g)} \quad (R5)$$

$$N_2O_{5(g)} + H_2O_{(aq)} \rightarrow 2HNO_{3(aq)} \quad (R6)$$

Air pollution is a global problem but needs local fixes (Li et al., 2019). Furthermore, accurately and effectively quantifying nitrate formation pathways and NO_x dominant sources are the initial steps towards local fixes. The measurement of isotope compositions in various emission sources, and the establishment of isotopic equilibrium fractionation equation, have provided theoretical bases for accurate source apportionment and transformation evaluation of nitrogen species. Isotope compositions in different sources were proved can provide valuable information in signal source attribution (Fang et al., 2011). For example, $\delta^{18}O$ values from O_3 and OH ranged from +90‰ to +122‰ and −15‰–0‰ respectively (Johnston and Thiemens, 1997; Zong et al., 2017; Krankowsky et al., 1995), while $\delta^{15}N$ value in different emission sources also varied in different ranges (Fig. S1, Text S1). The difference is that $\delta^{15}N$–NO_3^- is mostly emission source driven, but $\delta^{18}O$–NO_3^- is formation pathway driven (Zong et al., 2017). During the gas-to-particle conversion of NO_x to NO_3^-, the oxygen atoms of NO_3^- were mainly contributed by O_3 and OH, rather than the emission sources of NOx (Johnston and Thiemens, 1997; Krankowsky et al., 1995). Therefore, $\delta^{18}O$–NO_3^- features can be used to assess the contribution of NO_3^- convention pathways, and $\delta^{15}N$–NO_3^- was mostly used in the source apportionment of NO_x. These features above enable isotope composition to have distinct advantages in local source apportionment and formation pathway assessment than ground monitor system, remote sensing tools, satellite observation, air quality model, and emission inventory. Because the latter methods are more suitable for large-scale research, and usually has great uncertainty in local fixes and strong dependence on supporting data (Zong et al., 2017). Besides, isotope kinetic fractionation and equilibrium fractionation were normally reflected during the gas-to-particle conversion of NO_x to NO_3^-. Previous source apportionment of rainfall and particle nitrate by $\delta^{15}N$–NO_3^- usually underestimated or ignored N isotope fractionation values (Freyer, 2017; Felix and Elliott, 2014). The significant roles of isotope equilibrium fractionation during the gas-to-particle conversion of NO_x were recently re-emphasized (Chang et al., 2018), high fractionation values of 10.99‰ in the rural site and 15.33‰ in the urban site were respectively found, indicating the negligence of isotope effects may substantively miscalculate source contributions. By taking into account isotope kinetic fractionation, source contributions, and the importance of chemical pathways can be accurately and effectively quantified (Walters and Michalski, 2015).

As a heavy industry-based metropolis in Northeast China, Harbin was frequently plagued by haze pollution. Although haze pollution has been gradually alleviated under the adoption of political abatement, it is still far from eliminated. Precisely and effectively emission reduction on driving factors of $PM_{2.5}$; for instance, nitrate can further optimize emission abatement and control haze pollution. In this study, $PM_{2.5}$ sampling was conducted in urban Harbin from May-1, 2017 to April-30, 2018, isotopic composition ($\delta^{15}N$–NO_3^-, $\delta^{18}O$–NO_3^-) in fine particles were integrated with isotope fractionation module and Bayesian mixing model to explore NO_x dominant sources and oxidation pathways. This study focused mainly on the contrastive analysis between heating season (from mid-October to next mid-April) and non-heating season, also on the contrastive analysis between three pollution levels (as defined in

Table 1
Experimental constants of fractionation factors during the temperature range of 150 K–450 K.

$^m\alpha_{A/B}$	A	B	C	D	formulas
$^{15}NO_2/NO$	3.8834	−7.7299	6.0101	−0.17928	4
$^{15}N_2O_5/NO_2$	0.69398	−1.9859	2.3876	0.16308	5
$^{18}OH/H_2O$	2.1137	−3.8026	2.5653	0.59410	7
$^{18}NO_2/NO$	−0.04129	1.1605	−1.8829	0.74723	7

Sec. 3.1), aiming at providing scientific theoretical bases for NO_x reduction in urban Harbin and air quality improvement insights for other haze polluted regions in China.

2. Materials and methods

2.1. Sampling

The sampling campaign was conducted on the roof of a 5-floor building of Harbin Institute Technology (45°45′14″N, 126°40′54″E, approximately 15 m above the ground). A total of 85 ambient $PM_{2.5}$ samples were collected on quartz fiber filters (PALL, NY, U.S. 8 × 10 inch) using a high-volume sampler (Laoying, Qingdao, China). The sampling campaign was typically conducted every five days, or continuously during haze episodes. The flow rate and the sampling duration were set as 1.05 m^3 min^{-1} and 24-h (including 74 24-h samples (7:00 a.m. - next 7:00 a.m.), five night-samples (19:00 p.m. - 7:00 a.m.) and four day-samples (7:00 a.m. - 19:00 p.m.)). All filters were baked at 480 °C for 8-h before sampling and weighted at 0.1 mg accuracy. After sampling, filters were packaged in aluminum foil and sealed in polyethylene plastic bags, then stored at −20 °C for the downstream chemical analyses. We also collected gas pollutant data (carbon monoxide (CO), nitrogen dioxide (NO_2)) and meteorology data (temperature (T), relative humidity (RH), and wind speed (WS)) from the local air quality and meteorology monitoring station for further analysis (Fig. S3).

2.2. Chemical analysis and quality control

In this study, we extracted water-soluble ions (K^+, Ca^{2+}, Na^+, Mg^{2+}, NH_4^+, Cl^-, NO_3^-, F^- and SO_4^{2-}) using 20 ml ultrapure water, and 47 mm diameter discs which punched from quartz fiber filters. Then the extraction solution was detected by ion chromatograph (Dionex, Thermo scientific, Inc.U.S). Two reagents blank and one blank filter were conducted together with samples. The detection limit was 10–30 ng/ml, with the uncertainties <5%.

The $\delta^{15}N$ and $\delta^{18}O$ values of NO_3^- were analyzed by isotope ratio mass spectrometer (MAT253; Thermo Fisher Scientific, Waltham, MA, USA) after pre-treatment of cadmium reduction method (Tu et al., 2016). Firstly, 146.25 g NaCl, extracted solutions diluted to 15 μmol L^{-1} in 5 ml, 0.3 g cadmium powder (NaN_3), and 0.1 ml imidazole solution were put into reaction bottles. Then, sealed bottles were oscillated in an ultrasonic bath for 2-h at 40 °C, and sat quietly overnight. After that, 4 ml of supernatant was transferred to another bottle and reacted with 0.2 ml of sodium azide (1:1 of 20% acetic acid and sodium azide and purged with helium at 70 mL min^{-1} for 10 min) for 30 min in sealed and reversed reaction bottle. Finally, 0.4 ml of 10 M NaOH were injected into every bottle to stop the reaction. In the whole procession, NO_3^- was initially reduced to NO_2^- by cadmium powder, then further reduced to N_2O by sodium azide. N_2O was finally analyzed to get $\delta^{15}N$ and $\delta^{18}O$ values (‰).

$$\delta^{15}N(‰) = \left[\left({}^{15}N/{}^{14}N\right)_{sample} \Big/ \left({}^{15}N/{}^{14}N\right)_{standard} - 1\right] \times 1000 \quad (1)$$

$$\delta^{18}O(‰) = \left[\left({}^{18}O/{}^{16}O\right)_{sample} \Big/ \left({}^{18}O/{}^{16}O\right)_{standard} - 1\right] \times 1000 \quad (2)$$

Three international reference materials (USGS32, USGS34, and USGS35) were used for the calibration to air N_2. The standard deviation of the replicates was generally less than 0.68‰ for $\delta^{15}N$ and 0.82‰ for $\delta^{18}O$.

2.3. Isotope fractionation module and Bayesian mixing model

Bayesian mixing model (MixSIR) framework can usually generate robust probability estimates of multiple source contributions by explicitly taking into account uncertainty, the likelihood value, marginal probability distribution, prior information, as well as isotope fractionation (Moore and Semmens, 2008; Ward et al., 2010). In the process of simulation, the prior probability distribution of the source contribution was generated randomly first, and then sampling-importance - resampling was used to calculate the feasible solution and statistical distribution of contributions (Evans et al., 2000; Parnell et al., 2010) (detailed information was shown in Text S2).

Typically, Gas-to-particle conversion of NO_x to NO_3^- is related to thermodynamic equilibrium fractionation and kinetic disequilibrium fractionation (Walters and Michalski, 2015). Ignoring the isotope fractionation effect may incorrectly calculate source contributions (Chang et al., 2018). In this study, improved MixSIR with equilibrium/Leighton fractionation module by Zong et al. (2017) was introduced here to quantitatively assess multiple source contributions and conversion processes of NO_x-to-NO_3^-, the atmospheric nitrogen and oxygen isotope fractionation module were built by Zong et al. (2017) according to the approach by Walters et al. (2015) as follow (Walters and Michalski, 2015; Walters et al., 2016):

$$\delta^{15}N - NO_3^- = \gamma \times \left[O_H + (1+\gamma) \times \left[\delta^{15}N - NO_3^-\right]_{H_2O} = \gamma \times \left[O_H + (1-\gamma) \times \left[\delta^{15}N - HNO_3\right]_{H_2O}\right.\right. \quad (3)$$

The subscripts of OH and H_2O represent the pathway of OH oxidation and the pathway of N_2O_5 heterogeneous hydrolysis respectively, γ represents the contribution of OH oxidation pathway.

Isotope fractionation feature of OH pathway can be calculated using an approach:

$$\left[\delta^{15}N - HNO_3\right]_{OH} = 1000 \times \left[\frac{\left({}^{15}\alpha_{NO_2/NO}\right)\left(1 - f_{NO_2}\right)}{\left(1 - f_{NO_2}\right) + \left({}^{15}\alpha_{NO_2/NO} \times f_{NO_2}\right)}\right] \quad (4)$$

where ${}^{15}\alpha_{NO2/NO}$ is the nitrogen equilibrium fractionation factor between NO and NO_2, and f_{NO2} represents the fraction from NO_2 to NO_x. The fractionation feature of H_2O can be expressed as:

$$\left[\delta^{15}N - HNO_3\right]_{H_2O} = 1000 \times \left[{}^{15}\alpha_{N_2O_5/NO_2} - 1\right] \quad (5)$$

where ${}^{15}\alpha_{N2O5/NO}$ is the nitrogen equilibrium fractionation factor between N_2O_5 and NO_2. We assume that during the oxygen fractionation module, two-thirds and one-third oxygen in NO_2–OH pathways originate from O_3 and OH respectively. Correspondingly, five-six oxygen and one-six oxygen in N_2O_5–O_3 pathways way are respectively from O_3 and

OH. Similar to Eqs. (3)–(5), oxygen isotope fractionation effect from OH and H_2O pathways can be computed as follows:

$$\begin{aligned}\delta^{18}O-NO_3^- &= \gamma\times\left[\delta^{18}O-NO_3^-\right]_{OH}+(1-\gamma)\times\left[\delta^{18}O-NO_3^-\right]_{H_2O}\\ &= \gamma\times\left[\delta^{18}O-HNO_3\right]_{OH}+(1-\gamma)\times\left[\delta^{18}O-HNO_3\right]_{H_2O}\end{aligned} \quad (6)$$

$$\left[\delta^{18}O-HNO_3\right]_{OH}=\frac{2}{3}\left(\delta^{18}O-NO_2\right)+\frac{1}{3}\left(\delta^{18}O-OH\right)\ =\frac{2}{3}\left[\frac{1000\times\left({}^{18}\alpha_{NO_2/NO}-1\right)\left(1-f_{NO_2}\right)}{\left(1-f_{NO_2}\right)+\left({}^{18}\alpha_{NO_2/NO}\times f_{NO_2}\right)}\right]+\frac{1}{3}\left[\left(\delta^{18}O-H_2O\right)+1000\times\left({}^{18}\alpha_{OH/H_2O}-1\right)\right] \quad (7)$$

$$\left[\delta^{18}O-HNO_3\right]_{H_2O}=\frac{5}{6}\left(\delta^{18}O-N_2O_5\right)+\frac{1}{6}\left(\delta^{18}O-H_2O\right) \quad (8)$$

$$\delta^{18}O-NO_2=\delta^{18}O-N_2O_5=\delta^{18}O-O_3 \quad (9)$$

where ${}^{18}\alpha_{OH/H2O}$ is the oxygen equilibrium fractionation factor between OH and H_2O. The fractionation factors in Eqs. (4), (5) and (7) are all temperature-dependent functions, and their calculation formula and parameters are as follows (Walters et al., 2015, 2016; Walters and Michalski, 2015) (Table 1):

$$1000\times\left({}^{m}\alpha_{A/B}-1\right)=\frac{A}{T^4}\times10^{10}+\frac{B}{T^3}\times10^{8}+\frac{C}{T^2}\times10^{6}+\frac{D}{T}\times10^{4} \quad (10)$$

Based on the constants and Eqs. (6)–(8) above, γ was firstly generated by Monte Carlo simulation in this study, then γ was put into Eqs. (3)–(5) to generate the range of nitrogen fractionation factors. Here, coal combustion, biomass burning, vehicle emission, and biogenic emission were typical emission sources for simulation. Finally, temperature, isotope values, and typical emission source information were put into the MixSIR model to generate 10,000 feasible solutions. Source contributions were determined by $\delta^{15}N\text{-}NO_x$, which was transformed from $\delta^{15}N\text{–}NO_3^-$ using fractionation equation and formation pathways determined by oxygen isotope.

3. Result and discussion

3.1. Nitrate concentrations and isotope features in ambient $PM_{2.5}$

Before analysis, haze episodes were defined when daily $PM_{2.5}$ mass concentrations exceeding 75 μg/m^3, and 3 $PM_{2.5}$ pollution levels were divided according to the National Ambient Air Quality (NAAQ) standard (http://106.37.208.228:8082/) and previous studies (Wang and Liu, 2014; Zheng et al., 2016) (clean (C): $PM_{2.5}\leq75$ μg/m^3, slightly polluted (SP): 75< $PM_{2.5}$ ≤150 μg/m^3, heavily polluted (HP): $PM_{2.5}$ > 150 μg/m^3). Among all $PM_{2.5}$ samples collected in this study, 29 were collected in the non-heating season; the rest 56 samples were collected in heating season (Fig. 1), and the samples collected in C, SP, and HP were 27, 35 and 23 respectively. Shown as Fig. 1, $PM_{2.5}$ concentration ranged from 12.89 to 765.61 μg/m^3 during the study period (144.76 ± 134.26 μg/m^3). The non-heating season was dominated by clean days, and polluted days occasionally occurred, while the polluted days intensively occurred in heating season, which provide plentiful samples for haze characterization analysis and pollution cause exploration. Severe haze episodes were particularly prone to occur from late October to early November, with extremely striking $PM_{2.5}$ mass concentration and long duration time. During this period, coal-fired boilers were ignited, and dense fire points of biomass burning emerged around Harbin intensively (Fig. S2).

Fig. 2 illustrates the concentration and relative abundance of water-soluble ions in different $PM_{2.5}$ pollution levels. As expected, the concentration of all ionic profoundly increased as the pollution level elevated. Among which, the concentration of sulfate increased considerably, but its relative abundances decreased more considerably. On the contrary, the absolute concentration and relative abundance of nitrate, ammonium, chlorine, and potassium were all significantly enhanced, in particular, nitrate enhanced most. Thus, as one of the dominant contribution species, nitrate notably promoted the rapid build-up of $PM_{2.5}$ concentration than other water-soluble species. The average

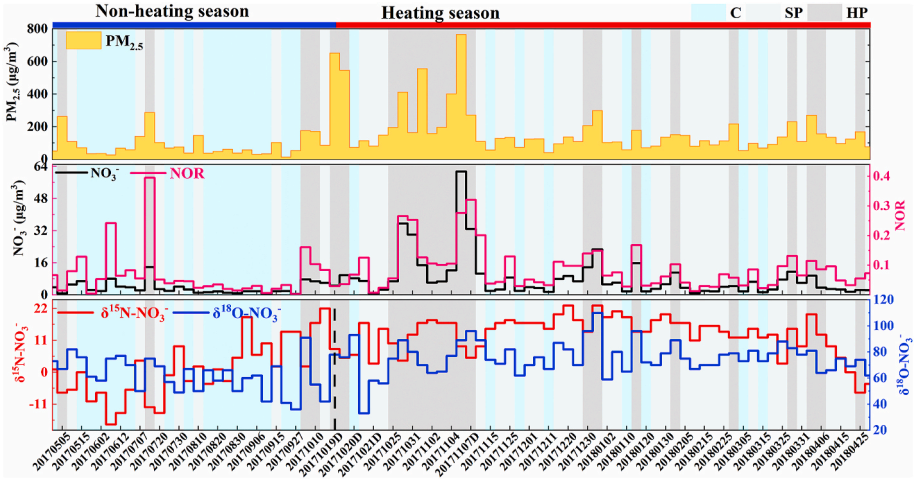

Fig. 1. The time series of NO_3^-, NOR, and isotope signatures ($\delta^{15}N\text{–}NO_3^-$, $\delta^{18}O\text{–}NO_3^-$) in ambient $PM_{2.5}$. (The color bar in the background represent three pollution levels with the same definition as Figs. 4a and 6c, blue: clean days; light gray: slightly polluted days; HP: heavily polluted days).

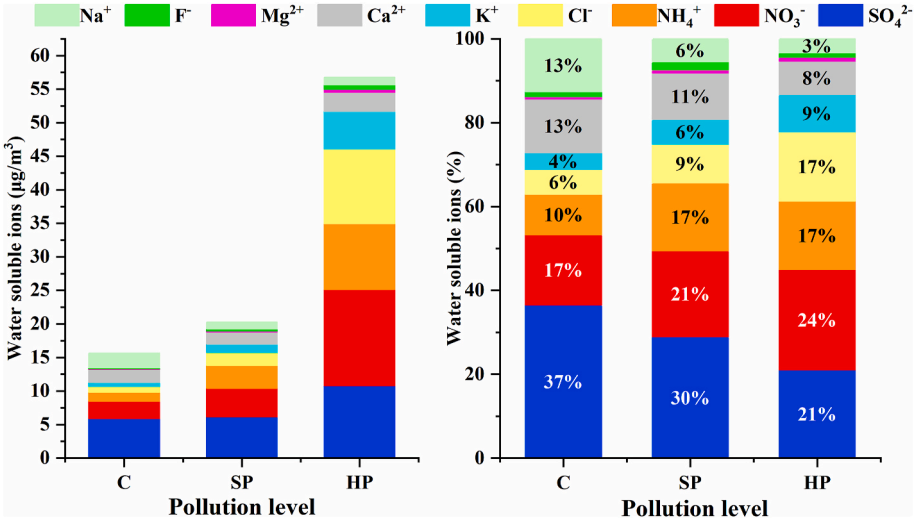

Fig. 2. Concentrations (left) and relative abundances (right) of water-soluble ionic species in different pollution levels.

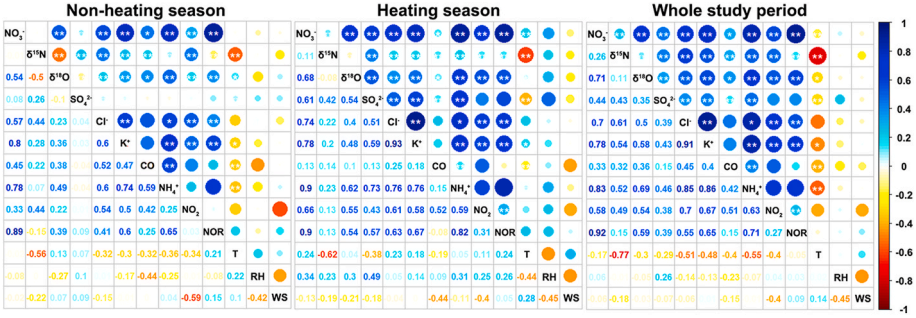

Fig. 3. The matrix of Spearman correlation coefficient between water-soluble species, isotope compositions, and meteorology parameters in non-heating season, heating season, and the whole study period. The bigger dots in the figure reflect higher correlation coefficients, and cool and warm color systems represent positive and negative correlation respectively. ** in the upper triangle represents the significance level less than 0.01, while * represents the significance level less than 0.05.

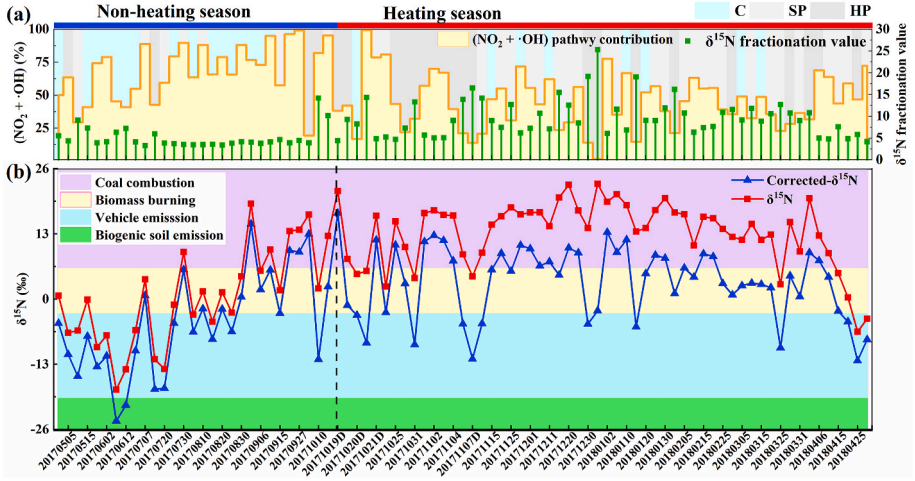

Fig. 4. Time series of the contribution of (NO_2 + OH) pathways (a), $\delta^{15}N$ fractionation value (a), and the corrected $\delta^{15}N$ values (b). The colored bands in Fig. 4b represent $\delta^{15}N$-NO_x ranges of four selected emission sources, as the legend illustrated. The detailed ranges were described in Fig. S1 and text S1.

concentration of NO_3^- significantly elevated in heating season (8.28 ± 10.18) than that in non-heating season (3.41 ± 2.98 μg/m^{3}μg/m^3), especially in October and November with the maximum value of 61.45 μg/m^3. In order to explore the in-depth causes, nitrogen oxidation ratios (NOR = $nNO_3^-/(nNO_3^- + nNO_2)$ (in mol)) was calculated to assess the conversion efficiency of atmospheric nitrogen to nitrate, the higher value of NOR indicates that more gaseous species would be oxidized to nitrate (Pearson, 1979; Sun et al., 2006). On average, NOR value in non-heating season (0.067 ± 0.081) was lower than that in heating season (0.086 ± 0.069). Similar to nitrate concentration and relative abundance, NOR increased as the elevation of pollution level (C: 0.046 ± 0.048, SP: 0.064 ± 0.039, HP: 0.140 ± 0.097), especially for HP,

which provides convincing evidence that nitrogen oxidation in haze episodes was significantly enhanced. Moreover, trace species that can provide important source information were selected in this study to initially and tentatively explore NO_x sources, including sulfate (SO_4^{2-}), chloride (Cl^-), non-sea-salt potassium (nss-K^+ = K^+ - 0.0035 × Na^+), carbon monoxide (CO), nitrogen dioxide (NO_2) and ammonia (NH_4^+). SO_4^{2-} is mainly related to coal combustion; Cl^- and nss-K^+ is considered as biomass burning tracers (Chang et al., 2018; Cao et al., 2016); CO is mostly completely derived from originated from incomplete combustion like traffic emission; while NH_4^+ is largely emitted by agriculture volatilization and fossil fuel combustion (Pan et al., 2016a,b; Chang et al., 2016). During the whole study period, NO_3^- was significantly correlated with NH_4^+, with the correlation coefficient in non-heating season and heating season of 0.74 and 0.91 respectively, indicating a good homology between them. Nitrate more strongly correlated with Cl (r = 0.75), nss-K^+ (r = 0.78), and SO_4^- (r = 0.61) in heating season than in non-heating season, suggesting extremely enhanced coal combustion and biomass burning emission. As shown in Fig. 3, NO_3^- and NOR seems insensitive to meteorological parameters. Thus, higher NO_3^- ($r_{NO3-,\ NO2}$ = 0.655) concentration and NOR ($r_{NOR,\ NO2}$ = 0.306) in heating season and polluted episodes were more likely attributed to enhanced NO_x emissions, because the correlation coefficient between NO_3^- (NOR) and trace species (SO_4^{2-}, Cl^-, nss-K^+, CO, NO_2 and NH_4^+) are generally higher than between meteorological parameters (T, RH, and WS) (Fig. 3, Table S2–S4).

$\delta^{15}N$–NO_3^- (without correction by fractionation factors) and $\delta^{18}O$–NO_3^- in this study ranged from −18.07‰ - 22.97‰ (8.82 ± 9.79‰) and 33.24‰–106.98‰ (70.87 ± 14.08‰) respectively. Overall, $\delta^{15}N$–NO_3^- varied seasonally with the lowest and highest values in June and January respectively (Fig. 1). The variation ranges of isotopes observed in this study varied wider than that of aerosol and rainfall samples in other studies, and the average values of isotope were also higher (Table S1). In general, $\delta^{15}N$–NO_3^- and $\delta^{18}O$–NO_3^- can reflect the information of emission sources and oxidation pathways (Fang et al., 2011; Zong et al., 2017; Felix and Elliott, 2014). Thus, the wide isotope variation in this study may be caused by more complicated NO_x emission sources and oxidation pathways during the whole period than in other studies, which may eventually be attributed to distinct temperature variations (from −30 to 30 °C generally) in Harbin. In this study, $\delta^{15}N$–NO_3^- significantly correlated with temperature (r = −0.756), but scarcely affected by other meteorology parameters and trace species, this result was consistent with other studies on $\delta^{15}N$–NO_3^- seasonal variation (Zong et al., 2017). $\delta^{18}O$–NO_3^- slightly fluctuated with opposite trends of $\delta^{15}N$–NO_3^- in this study, especially in clean days. $\delta^{18}O$–NO_3^- also correlated with temperature, but was more predominantly associated with NOR and NO_3^-, because $\delta^{18}O$–NO_3^- was modulated solely by O isotope exchange reactions (Zong et al., 2017).

3.2. *Nitrate formation pathways assessment and $\delta^{15}N$–NO_3^- correction based on isotope fractionation module*

In Fig. 4, the time series of the mean contribution of OH pathway was displayed, which assessed by isotope fractionation module and Monte Carlo simulation. A sharp contrast of the contribution of OH pathway between heating season and non-heating season can be observed in Fig. 4. OH conversion pathways dominants non-heating season with an average fraction of 67.34%, while in heating season were only 45.24%. Thus, the primary oxidation agents for NO_x in non-heating season and heating season were homogeneous (NO_2–OH) and heterogeneous (N_2O_5–O_3 pathways) respectively. As illustrated in Fig. 5, the contributions of NO_2–OH pathways and N_2O_5 - O_3 pathways in day samples, night samples, and three pollution levels were counted, from which a clear stepped downward trend of the contribution of NO_2–OH pathways was observed as pollution level elevated, and a much lower fraction of contribution of NO_2–OH pathways in nighttime was observed. Conversely, the importance of O_3 oxidization and N_2O_5 heterogeneous hydrolysis was more prominent in severer haze episodes (C: 35.41% ± 19.76%, SP: 45.36% ± 22.29%, HP: 62.95% ± 21.16%) and nigh-time (63.91% ± 26.00%). These results above consist with nitrate formation pathways observed in previous studies that OH oxidization pathways (R3) were reported more prevalent during daytime and summer, while O_3 oxidization and N_2O_5 heterogeneous hydrolysis (R4–R6) mostly occurred overnight and winter (Altieri et al., 2013; Fang et al., 2011). Generally, the high temperature was reported conducive to the

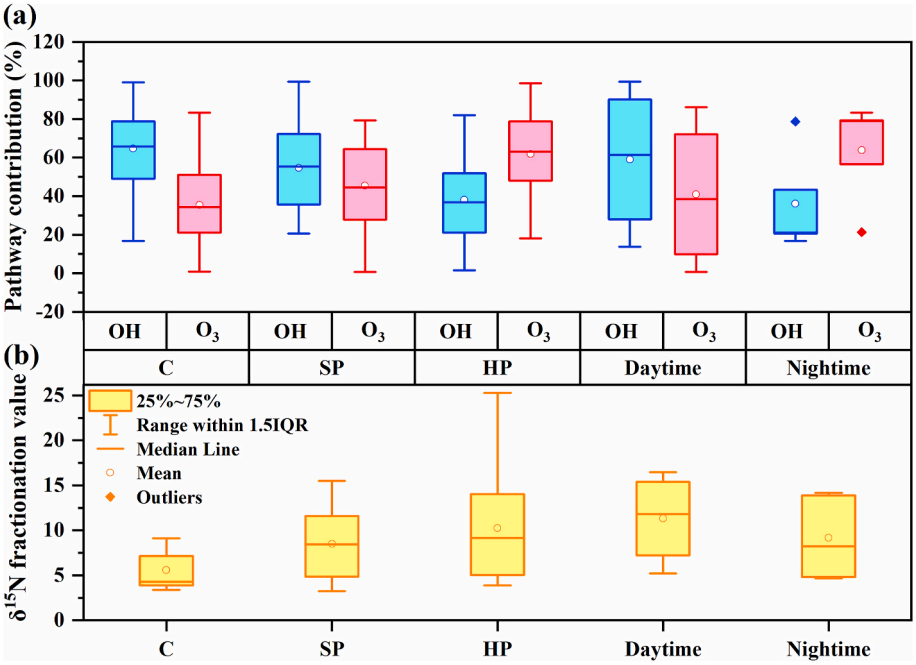

Fig. 5. Boxplot of the contribution of NO_2–OH pathway and N_2O_5–O_3 pathway (a), and $\delta^{15}N$ fractionation value (b) respectively in the daytime, nighttime, and three pollution levels. OH and O_3 in the figure represent NO_2–OH pathway and N_2O_5–O_3 pathway respectively. C, SP, and HP were the abbreviation of clean days, slightly polluted days, and heavily polluted days.

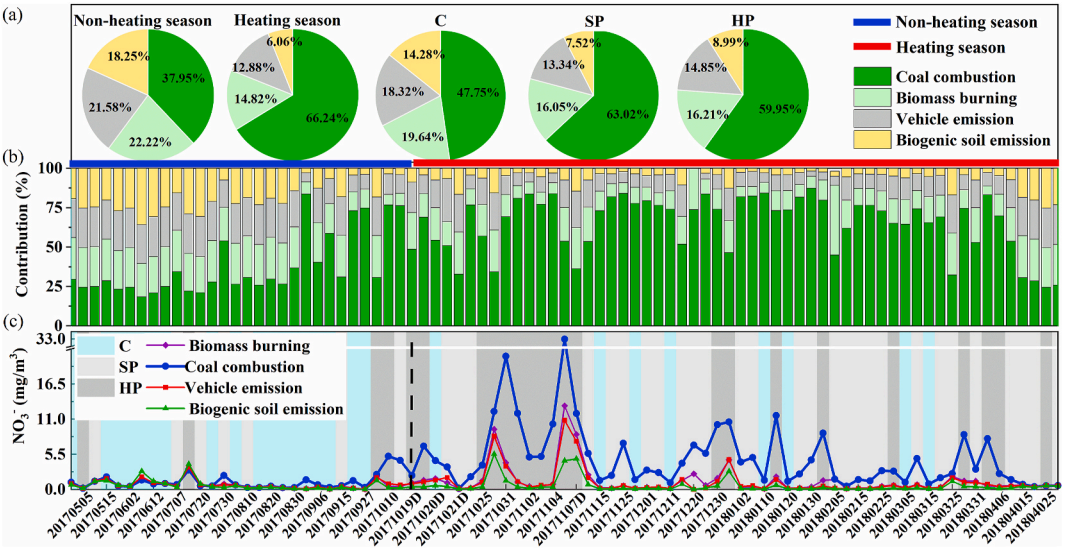

Fig. 6. Source contributions in non-heating season, heating season and different pollution level (a); Time series of the relative contributions of four selected emission sources (b); Time series of sources related NO_3^- concentrations (c) (which were the product of the measured nitrate concentrations and source contributions).

formation of HO·. Thus HO· is more abundant in summer than in winter, and that HO· was reported mainly formed by photolysis of ozone in clean days, while mainly formed by photolysis of nitrous acid and hydrogen in polluted atmospheric environment (Altieri et al., 2013; Calvert et al., 1985). Thus higher NO_2–OH pathways contribution in the daytime can be ascribed to higher temperatures. For O_3, its formation rate and decomposition rate in the ozonosphere in clean days are basically equal; thus, its amount keeps in an equilibrium state (Lu et al., 2019; von Tiedemann and Firsching, 2000). However, in polluted days, excessive discharged volatile organic compounds (VOCs) and subsequently generated radicals destroyed this equilibrium state, lead to ozone gradually accumulated to polluted level (Li et al., 2019; Lu et al., 2019). Furthermore, weakened radiation and photochemistry reaction, but enhanced heterogeneous hydrolysis in severe haze episodes was also revealed by recent researches (Zheng et al., 2015, 2016). Stated thus, neither the low temperature nor the weakened photochemistry reaction was conducive to OH generation pathways in heating season, but provide convenience for N_2O_5–O_3 pathways. The investigation of nitrate formation pathways in this study revealed that O_3 pollution alleviation has a priority significance for mitigating atmospheric nitrate and haze pollution in heating season and severe polluted episodes.

$\delta^{15}N$ fractionation value calculated by isotope fractionation module ranged from 3.23‰ to 25.29‰, also has much higher value in heating season and severer haze episodes than that in clean days (C: 5.57‰ ± 2.06‰, SP: 8.50‰ ± 3.53‰, HP: 10.24‰ ± 5.86‰). An obvious elevation of $\delta^{15}N$ fractionation value after 19-Oct is clearly visible (Fig. 4), implying more significant $\delta^{15}N$ isotope partitioning occurred in heating season. Notably, a significant Spearman correlation coefficient between $\delta^{15}N$ fractionation value and N_2O_5–O_3 pathway contribution ($r = 0.688$, p-value = 0) was also observed, demonstrating that complex conversion pathway of N_2O_5–O_3 leading to higher isotope fractionation effect, in particular of in haze episodes. Generally, NO_x from coal combustion (13.77‰ ± 4.50‰) and biomass burning (1.04‰ ± 4.13‰) usually have higher $\delta^{15}N$ values, while from vehicle emission (−7.25‰ ± 7.77‰) and biogenic soil emissions (−33.77‰ ± 12.16‰) have relatively lower values (Fig. S1). Thus, the increasing trend of $\delta^{15}N$–NO_3^- values in heating season compared to non-heating season (Fig. 4), and the negative correlation between $\delta^{15}N$–NO_3^- values and temperature (Fig. 3) can be most likely interpreted by increased coal combustion and biomass burning emission in winter contributed high $\delta^{15}N$–NO_3^- values. On the contrary, biogenic soil emissions that contributed low $\delta^{15}N$–NO_3^- values were decreased in heating season, because of decreased nitrification and denitrification of soil microorganisms under cold temperature (Eriksson et al., 2003). Illustrated by Fig. 4, corrected $\delta^{15}N$–NO_3^- values mostly fall within the scope of vehicle emission and biogenic soil emission in non-heating season, and within the scope of coal combustion and biomass burning in heating season, which is consistent well with the tentative exploration of NO_3^- sources as mention above, which enormously avoiding the overestimation of the contribution of coal combustion.

3.3. NOx sources apportionment

As described above, four major NO_x sources were integrated into MixSIR, and the dynamic variations of their contribution were quantified based on the corrected $\delta^{15}N$–NO_3^-. As illustrated in Fig. 6 (a), coal combustion was the dominant contributor to NO_x in urban Harbin, with a significant high relative contribution of 55.67% ± 22.60% throughout the whole study period, even if in non-heating season, the average contribution of coal combustion still ranked first (37.95% ± 27.16%), but this is far lower than the predominant high value of 66.24% ± 17.94% in heating season. These findings differed from previous studies in Southern China, that the NO_x emitted by road traffic is twice as much as coal combustion, and high NO_x was typically found from massive emission of mobile sources (gasoline and diesel fuel) (Wang et al., 2006; Chang et al., 2018). Nevertheless, the results in this study consist of some research in Northern China, like Beihuangcheng Island and Xuzhou, that coal combustion was the largest NO_x contributor in winter (Fan et al., 2019; Zong et al., 2017). The divergence of energy structure and emission system between South China and North China may be responsible for such a difference. In the last few years, auto sales in China experienced continuous growth and gradually ascended into world's largest automobile market, in particular of in densely populated and economically developed cities (Chang et al., 2018, 2019; Liu et al., 2013). Meanwhile, old-fashioned and small power plants were gradually phased out. The economic change above eventually led to traffic-related NOx emissions surpassing coal-fired emissions in most Southern China cities. This view was also confirmed by a continuously increasing NO_3^-/SO_4^{2-} ratio from long-term measurements (Liu et al., 2013). In North China, the low ambient temperature in winter resulted in large amounts of coal-fired heating was the major contributor to atmospheric pollution. As the coldest and Northernmost capital city of China, Harbin ranked the largest land area (10,200 km^2) and the third-largest registered population (5.5 million) among all provincial capitals in China

(Chen et al., 2018). It was also strongly governed by Siberian Cold Current in its long heating seasons (nearly half year from Mid-October to next mid-April). Cold weather and large residential users in winter determine a large amount of heating demand and intensive coal-fired emission. From Fig. 6b, coal combustion contribution sharply increased from October, afterward maintained a relatively high value until the next April. Although central heating and industrial emission reduction were positively promoted and vigorously implemented by the government, the dominant status of coal combustion emission reflected by this study was still not changed. Thus, coal combustion should be targeted in plans to reduce NO_x emissions. Coal combustion in non-heating season basically emits equal NO_x emissions with other sources, only with few high values were observed (Fig. 6b), the contribution in this period can be most likely attribute to power plants emissions (Sun et al., 2020; Fan et al., 2019). Shown as Fig. 6 (a, c), the contribution of coal combustion in polluted was higher than that in clean days, and coal combustion related NO_3^- concentrations in heavily polluted days were the most predominant. Given the importance of nitrate during haze evolution and the dominant contribution of coal combustion to NO_x in polluted days, reducing coal combustion appears to be one further crucial work to take for mitigating nitrate pollution in the urban area of Harbin. Therefore, more efforts for coal quality improvement, scattered coal combustion management, and clean energy promotion should be implemented.

The other three NO_x contributors with the order of importance were biomass burning (17.81% ± 7.96%), mobile sources (15.93% ± 7.59%), and biogenic soil emissions (10.57% ± 8.97%) respectively. Their contributions declined in heating season and rebounded in non-heating season. The contribution of biomass burning is close to but slightly higher than that of vehicle emission. The region Harbin belonged was renowned for many times due to fertile land and well-developed agriculture (Chen et al., 2017). Agricultural residues burning during harvesting season is accepted as one of the most effective ways to reduce straw accumulation (Cao et al., 2016; Qin et al., 2014). Given the significant contribution of biomass combustion to air pollution, some efforts and new emission standards are required to reduce biomass fuel boilers and agriculture waste burning. Biogenic soil contributed minimal impact to ambient NO_x in heating season (6.06% ± 5.63%), but its contribution rebounded in non-heating season, which was consistent with plentiful rainfall in non-heating season (almost 60% precipitation in Harbin focused in summer). Generally, biogenic emission was considered should keep at a low level in winter because of decreased microbial activity, and vehicle emission should keep at a stable level. But from Fig. 6c, during polluted episodes, NO_x amounts from four sources were simultaneously enhanced, in particular in the severest and longest haze pollution from 25-Oct to 7-Nov. Adverse weather systems such as reduced surface wind speed promoted air mass-sinking motion, enhanced stability, suppressed planetary boundary layer height, and induced humid and warm advection may play essential roles in modulating source related NO_x concentrations. The developed temperature inversion layer acted as a lid to suppress vertical diffusion, and adverse horizontal diffusion conditions favored the accumulation of pollutants along the horizontal scale (Ning et al., 2018; Luo et al., 2018). Thus, even if the NO_x emission rates from four sources kept at a relatively stable level, their emission amounts in the atmospheric environment would be simultaneously accumulated.

4. Conclusion

To give hints about the dominant sources of nitrogen oxide and the formation pathways of particulate nitrate in urban Harbin, one-year $\delta^{15}N–NO_3^-$ and $\delta^{18}O–NO_3^-$ from $PM_{2.5}$ samples were measured, and improved Bayesian mixing model was introduced in this study. From the results, three crucial findings were demonstrated. Firstly, nitrate was observed notably promoted the rapid build-up of $PM_{2.5}$ concentration in heating season. Meanwhile, nitrate was found strongly correlated with trace species but was insensitive to meteorological parameters. Secondly, coupling the isotope fractionation module and isotope signatures, the results suggested that considering $\delta^{15}N$ fractionation value could largely avoid the miscalculation of the source contribution of nitrogen oxide, especially for samples at high pollution level and daytime. From the module, this study also observed that homogeneous reaction and heterogeneous reaction were the dominant conversion pathways of NO_x to NO_3^- in non-heating season and heating season respectively, and the contribution of heterogeneous reaction increased as pollution levels increased. Thirdly, this study made use of MixSIR to address the source apportionment of atmospheric NO_x with regards to $\delta^{15}N$ fractionation value. Eventually, coal combustion was calculated as the dominant contributor to NO_x, which mostly related to power plants in non-heating season and related to heating system in heating season. The other three targeted contributors to NO_x emission with the order of importance were biomass burning, mobile sources, and biogenic soil emissions, which played relatively minor roles in atmospheric nitrate. Our finding shed light on the dominant role of coal combustion and heterogeneous reaction for nitrate formation in severe haze episodes, also emphasized the critical importance in terms of adapting suitable mitigation measures, which may provide scientific theoretical bases for NO_x reduction and air quality improvement insights for haze polluted regions.

Declaration of competing interest

The authors declare that they have no known competing financial interests or personal relationships that could have appeared to influence the work reported in this paper.

Acknowledgement

This work was supported financially by the National Science Foundation of China (51979066) and the State Key Laboratory of Urban Water Resource and Environment Funding, Harbin Institute of Technology (No. HC201811).

Appendix A. Supplementary data

Supplementary data to this article can be found online at https://doi.org/10.1016/j.polymer.2020.117730.

References

Alexander, B., Hastings, M.G., Allman, D.J., Dachs, J., Thornton, J.A., Kunasek, S.A., 2009. Quantifying atmospheric nitrate formation pathways based on a global model of the oxygen isotopic composition (delta O-17) of atmospheric nitrate. Atmos. Chem. Phys. 9, 5043–5056. https://doi.org/10.5194/acp-9-5043-2009.

Altieri, K.E., Hastings, M.G., Gobel, A.R., Peters, A.J., Sigman, D.M., 2013. Isotopic composition of rainwater nitrate at Bermuda: the influence of air mass source and chemistry in the marine boundary layer. J. Geophys. Res. Atmos. 118, 11304–11316. https://doi.org/10.1002/jgrd.50829.

Brauer, M., Freedman, G., Frostad, J., van Donkelaar, A., Martin, R.V., Dentener, F., van Dingenen, R., Estep, K., Amini, H., Apte, J.S., Balakrishnan, K., Barregard, L., Broday, D., Feigin, V., Ghosh, S., Hopke, P.K., Knibbs, L.D., Kokubo, Y., Liu, Y., Ma, S., Morawska, L., Sangrador, J.L., Shaddick, G., Anderson, H.R., Vos, T., Forouzanfar, M.H., Burnett, R.T., Cohen, A., 2016. Ambient air pollution exposure estimation for the global burden of disease 2013. Environ. Sci. Technol. 50, 79–88. https://doi.org/10.1021/acs.est.5b03709.

Calvert, J.G., Lazrus, A., Kok, G.L., Heikes, B.G., Walega, J.G., Lind, J., Cantrell, C.A., 1985. Chemical mechanisms of acid generation in the troposphere. Nature 317, 27–35.

Cao, F., Zhang, S., Kawamura, K., Zhang, Y., 2016. Inorganic markers, carbonaceous components and stable carbon isotope from biomass burning aerosols in Northeast China. Sci. Total Environ. 572, 1244–1251. https://doi.org/10.1016/j.scitotenv.2015.09.099.

Chang, Y., Liu, X., Deng, C., Dore, A.J., Zhuang, G., 2016. Source apportionment of atmospheric ammonia before, during, and after the 2014 APEC summit in Beijing using stable nitrogen isotope signatures. Atmos. Chem. Phys. Discuss. 1–26, 10.5194/acp-2016-432.

Chang, Y., Zhang, Y., Li, J., Tian, C., Song, L., Zhai, X., Zhang, W., Huang, T., Lin, Y., Zhu, C., Fang, Y., Lehmann, M.F., Chen, J., 2019. Isotopic constraints on the atmospheric sources and formation of nitrogenous species in clouds influenced by

biomass burning. Atmos. Chem. Phys. 19, 12221–12234. https://doi.org/10.5194/acp-19-12221-2019.
Chang, Y., Zhang, Y., Tian, C., Zhang, S., Ma, X., Cao, F., Liu, X., Zhang, W., Kuhn, T., Lehmann, M.F., 2018. Nitrogen isotope fractionation during gas-to-particle conversion of NO_x to NO_3^- in the atmosphere–implications for isotope-based NO_x source apportionment. Atmos. Chem. Phys. 18, 11647–11661. https://doi.org/10.5194/acp-18-11647-2018.
Chen, Q., Yuan, Y., Huang, X., He, Z., Tan, H., 2018. Assessment of column aerosol optical properties using ground-based sun-photometer at urban Harbin, Northeast China. J Environ Sci-China 74, 50–57. https://doi.org/10.1016/j.jes.2018.02.003.
Chen, W., Tong, D.Q., Dan, M., Zhang, S., Zhang, X., Pan, Y., 2017. Typical atmospheric haze during crop harvest season in northeastern China: a case in the Changchun region. J Environ Sci-China 54, 101–113. https://doi.org/10.1016/j.jes.2016.03.031.
Eriksson, P.G., Svensson, J.M., Carrer, G.M., 2003. Temporal changes and spatial variation of soil oxygen consumption, nitrification and denitrification rates in a tidal salt marsh of the Lagoon of Venice, Italy, Estuarine. Coast. Shelf Sci. 58, 861–871. https://doi.org/10.1016/j.ecss.2003.07.002.
Evans, J., Handley, S.J., Perham, N., Over, D.E., Thompson, V.A., 2000. Frequency versus Probability Formats in Statistical Word Problems. Cognition 77, 197–213. https://doi.org/10.1016/S0010-0277(00)00098-6.
Fan, M., Zhang, Y., Lin, Y., Chang, Y., Cao, F., Zhang, W., Hu, Y., Bao, M., Liu, X., Zhai, X., Lin, X., Zhao, Z., Song, W., 2019. Isotope-based source apportionment of nitrogen-containing aerosols: a case study in an industrial city in China. Atmos. Environ. 212, 96–105. https://doi.org/10.1016/j.atmosenv.2019.05.020.
Fang, Y.T., Koba, K., Wang, X.M., Wen, D.Z., Li, J., Takebayashi, Y., Liu, X.Y., Yoh, M., 2011. Anthropogenic imprints on nitrogen and oxygen isotopic composition of precipitation nitrate in a nitrogen-polluted city in southern China. Atmos. Chem. Phys. 11, 1313–1325. https://doi.org/10.5194/acp-11-1313-2011.
Felix, J.D., Elliott, E.M., 2014. Isotopic composition of passively collected nitrogen dioxide emissions: vehicle, soil and livestock source signatures. Atmos. Environ. 92, 359–366. https://doi.org/10.1016/j.atmosenv.2014.04.005.
Freyer, H.D., 2017. Seasonal trends of NH_4^+ and NO_3^- nitrogen isotope composition in rain collected at Jülich, Germany. Tellus 43, 30–44. https://doi.org/10.3402/tellusb.v43i1.15244.
Galloway, J.N., Aber, J.D., Erisman, J.W., Seitzinger, S.P., Howarth, R.W., Cowling, E.B., Cosby, B.J., 2003. The nitrogen cascade. Bioscience 53, 341–356.
Gu, B., Ge, Y., Ren, Y., Xu, B., Luo, W., Jiang, H., Gu, B., Chang, J., 2012. Atmospheric reactive nitrogen in China: sources, recent trends, and damage costs. Environ. Sci. Technol. 46, 9420–9427. https://doi.org/10.1021/es301446g.
Gu, B., Ju, X., Chang, J., Ge, Y., Vitousek, P.M., 2015. Integrated reactive nitrogen budgets and future trends in China. Proc. Natl. Acad. Sci. Unit. States Am. 112, 8792–8797. https://doi.org/10.1073/pnas.1510211112.
Johnston, J.C., Thiemens, M.H., 1997. The isotopic composition of tropospheric ozone in three environments. J. Geophys. Res. Atmos. 102, 25395–25404. https://doi.org/10.1029/97JD02075.
Krankowsky, D., Barcekti, F., Klees, G.G., Mauersberger, K., Schellenbach, K., Stehr, J., 1995. Measurement of heavy isotope enrichment in tropospheric ozone. Geophys. Res. Lett. 22, 1713–1716. https://doi.org/10.1029/95GL01436.
Lelieveld, J., Barlas, C., Giannadaki, D., Pozzer, A., 2013. Model calculated global, regional and megacity premature mortality due to air pollution. Atmos. Chem. Phys. 13, 7023–7037. https://doi.org/10.5194/acp-13-7023-2013.
Li, K., Jacob, D.J., Liao, H., Zhu, J., Shah, V., Shen, L., Bates, K.H., Zhang, Q., Zhai, S., 2019. A two-pollutant strategy for improving ozone and particulate air quality in China. Nat. Geosci. 12 (906) https://doi.org/10.1038/s41561-019-0464-x.
Li, L., Tan, Q., Zhang, Y., Feng, M., Qu, Y., An, J., Liu, X., 2017. Characteristics and source apportionment of $PM_{2.5}$ during persistent extreme haze events in Chengdu, southwest China. Environ. Pollut. 230, 718–729. https://doi.org/10.1016/j.envpol.2017.07.029.
Li, X., Jin, L., Kan, H., 2019. Air pollution: a global problem needs local fixes. Nature 570.
Liu, M., Huang, X., Song, Y., Tang, J., Cao, J., Zhang, X., Zhang, Q., Wang, S., Xu, T., Kang, L., Cai, X., Zhang, H., Yang, F., Wang, H., Yu, J.Z., Lau, A.K.H., He, L., Huang, X., Duan, L., Ding, A., Xue, L., Gao, J., Liu, B., Zhu, T., 2019. Ammonia emission control in China would mitigate haze pollution and nitrogen deposition, but worsen acid rain. P Natl Acad Sci Usa 116, 7760–7765. https://doi.org/10.1073/pnas.1814880116.
Liu, X., Zhang, Y., Han, W., Tang, A., Shen, J., Cui, Z., Vitousek, P., Erisman, J.W., Goulding, K., Christie, P., Fangmeier, A., Zhang, F., 2013. Enhanced nitrogen deposition over China. Nature 494, 459–462. https://doi.org/10.1038/nature11917.
Lu, X., Zhang, L., Chen, Y., Zhou, M., Zheng, B., Li, K., Liu, Y., Lin, J., Fu, T., Zhang, Q., 2019. Exploring 2016–2017 surface ozone pollution over China: source contributions and meteorological influences. Atmos. Chem. Phys. 19, 8339–8361. https://doi.org/10.5194/acp-19-8339-2019.
Luo, M., Hou, X., Gu, Y., Lau, N., Yim, S.H., 2018. Trans-boundary air pollution in a city under various atmospheric conditions. Sci. Total Environ. 618, 132–141. https://doi.org/10.1016/j.scitotenv.2017.11.001.
Moore, J.W., Semmens, B.X., 2008. Incorporating uncertainty and prior information into stable isotope mixing models. Ecol. Lett. 11, 470–480. https://doi.org/10.1111/j.1461-0248.2008.01163.x.
Ning, G., Wang, S., Yim, S.H.L., Li, J., Hu, Y., Shang, Z., Wang, J., Wang, J., 2018. Impact of low-pressure systems on winter heavy air pollution in the northwest Sichuan Basin, China. Atmos. Chem. Phys. 18, 13601–13615. https://doi.org/10.5194/acp-18-13601-2018.
Pan, Y., Tian, S., Liu, D., Fang, Y., Zhu, X., Zhang, Q., Zheng, B., Michalski, G., Wang, Y., 2016a. Fossil fuel combustion-related emissions dominate atmospheric ammonia sources during severe haze episodes: evidence from15N-stable isotope in size-resolved aerosol ammonium. Environ. Sci. Technol. 50, 8049–8056. https://doi.org/10.1021/acs.est.6b00634.
Pan, Y., Wang, Y., Zhang, J., Liu, Z., Wang, L., Tian, S., Tang, G., Gao, W., Ji, D., Song, T., Wang, Y., 2016b. Redefining the importance of nitrate during haze pollution to help optimize an emission control strategy. Atmos. Environ. 141, 197–202. https://doi.org/10.1016/j.atmosenv.2016.06.035.
Parnell, A.C., Inger, R., Bearhop, S., Jackson, A.L., 2010. Source partitioning using stable isotopes: coping with too much variation. PloS One 5. https://doi.org/10.1371/journal.pone.0009672.
Pearson, W.R.B.W., 1979. Sulfate emissions from catalyst-equipped automobiles on the highway. Air Repair 3, 255–257.
Qin, X., Yan, H., Zhan, Z., Li, Z., 2014. Characterising vegetative biomass burning in China using MODIS data. Int. J. Wildland Fire 23, 69. https://doi.org/10.1071/WF12163.
Sun, X., Wang, K., Li, B., Zong, Z., Shi, X., Ma, L., Fu, D., Thapa, S., Qi, H., Tian, C., 2020. Exploring the cause of $PM_{2.5}$ pollution episodes in a cold metropolis in China. J. Clean. Prod. 256.
Sun, Y., Zhuang, G., Tang, A., Wang, Y., An, Z., 2006. Chemical characteristics of $PM_{2.5}$ and PM_{10} in haze-fog episodes in Beijing. Environ. Sci. Technol. 40, 3148–3155. https://doi.org/10.1021/es051533g.
Tu, Y., Fang, Y., Liu, D., Pan, Y., 2016. Modifications to the azide method for nitrate isotope analysis. Rapid Commun. Mass Spectrom. 30, 1213–1222. https://doi.org/10.1002/rcm.7551.
Vienne, C., Errard, C., Lenoir, A., 1961. Photochemistry of Air Pollution.
von Tiedemann, A., Firsching, K.H., 2000. Interactive effects of elevated ozone and carbon dioxide on growth and yield of leaf rust-infected versus non-infected wheat. Environ. Pollut. 108, 357–363.
Walters, W.W., Simonini, D.S., Michalski, G., 2016. Nitrogen isotope exchange between NO and NO_2 and its implications for $\delta^{15}N$ variations in tropospheric NO_x and atmospheric nitrate. Geophys. Res. Lett. 43, 440–448. https://doi.org/10.1002/2015GL066438.
Walters, W.W., Tharp, B.D., Fang, H., Kozak, B.J., Michalski, G., 2015. Nitrogen isotope composition of thermally produced NO_x from various fossil-fuel combustion sources. Environ. Sci. Technol. 49, 11363–11371. https://doi.org/10.1021/acs.est.5b02769.
Walters, W.W., Michalski, G., 2015. Theoretical calculation of nitrogen isotope equilibrium exchange fractionation factors for various NO y molecules. Geochem. Cosmochim. Acta 164, 284–297. https://doi.org/10.1016/j.gca.2015.05.029.
Wang, H., Lu, K., Chen, X., Zhu, Q., Chen, Q., Guo, S., Jiang, M., Li, X., Shang, D., Tan, Z., Wu, Y., Wu, Z., Zou, Q., Zheng, Y., Zeng, L., Zhu, T., Hu, M., Zhang, Y., 2017. High N_2O_5 concentrations observed in urban Beijing: implications of a large nitrate formation pathway. Environ. Sci. Technol. Lett. 4, 416–420. https://doi.org/10.1021/acs.estlett.7b00341.
Wang, K., Liu, Y., 2014. Can Beijing fight with haze? Lessons can be learned from London and los angeles. Nat. Hazards 72, 1265–1274. https://doi.org/10.1007/s11069-014-1069-8.
Wang, Y., Zhuang, G., Zhang, X., Huang, K., Xu, C., Tang, A., Chen, J., An, Z., 2006. The ion chemistry, seasonal cycle, and sources of $PM_{2.5}$ and TSP aerosol in Shanghai. Atmos. Environ. 40, 2935–2952. https://doi.org/10.1016/j.atmosenv.2005.12.051.
Ward, E.J., Semmens, B.X., Schindler, D.E., 2010. Including source uncertainty and prior information in the analysis of stable isotope mixing models. Environ. Sci. Technol. 44, 4645–4650.
Whiteman, C.D., Hoch, S.W., Horel, J.D., Charland, A., 2014. Relationship between particulate air pollution and meteorological variables in Utah's Salt Lake Valley. Atmos. Environ. 94, 742–753. https://doi.org/10.1016/j.atmosenv.2014.06.012.
Xiao, H., Xie, L., Long, A., Ye, F., Pan, Y., Li, D., Long, Z., Chen, L., Xiao, H., Liu, C., 2015. Use of isotopic compositions of nitrate in TSP to identify sources and chemistry in South China Sea. Atmos. Environ. 109, 70–78. https://doi.org/10.1016/j.atmosenv.2015.03.006.
Zheng, G., Duan, F., Ma, Y., Zhang, Q., Huang, T., Kimoto, T., Cheng, Y., Su, H., He, K., 2016. Episode-based evolution pattern analysis of haze pollution: method development and results from Beijing, China. Environ. Sci. Technol. 50, 4632–4641. https://doi.org/10.1021/acs.est.5b05593.
Zheng, G.J., Duan, F.K., Su, H., Ma, Y.L., Cheng, Y., Zheng, B., Zhang, Q., Huang, T., Kimoto, T., Chang, D., Pöschl, U., Cheng, Y.F., He, K.B., 2015. Exploring the severe winter haze in Beijing: the impact of synoptic weather, regional transport and heterogeneous reactions. Atmos. Chem. Phys. 15, 2969–2983. https://doi.org/10.5194/acp-15-2969-2015.
Zong, Z., Wang, X., Tian, C., Chen, Y., Fang, Y., Zhang, F., Li, C., Sun, J., Li, J., Zhang, G., 2017. First assessment of NO_x sources at a regional background site in North China using isotopic analysis linked with modeling. Environ. Sci. Technol. 51, 5923–5931. https://doi.org/10.1021/acs.est.6b06316.